Phase Separation Mechanism of Polybutadiene/Polyisoprene Blends under Oscillatory Shear Flow

Ruoyu Zhang,[†,‡] He Cheng,[†] Chenggui Zhang,[§] Tongchen Sun,[†,‡] Xia Dong,*[,†] and Charles C. Han*[,†]

Beijing National Laboratory for Molecular Sciences, Joint Laboratory of Polymer Science and Materials, State Key Laboratory of Polymer Physics and Chemistry, Institute of Chemistry, Chinese Academy of Sciences, Beijing 100190, China; Graduate School of the Chinese Academy of Sciences, Beijing 100049, China; and School of Material and Chemical Engineering, Zhengzhou University of Light Industry, Zhengzhou 450002, China

Received March 23, 2008; Revised Manuscript Received May 18, 2008

ABSTRACT: Viscoelastic polymer blends of polybutadiene (PB)/low vinyl content polyisoprene (LPI), with a lower critical solution temperature (LCST), show interesting rheological behaviors in temperature ramp measurements. In this report, a systematic study has been carried out, and the underlying physics has been investigated for the storage modulus G' at various temperatures and shear frequencies as the system passes through the binodal and the spinodal phase boundary lines. We considered the nucleation mechanism, spinodal fluctuations, shear induced mixing, and rheological models in the interpretation of these interesting phenomena. Shear induced mixing is varied in our system, and the frequency dependence is obvious. Competition between the kinetics of the nucleation process and the droplet growth process has a prominent effect on the storage modulus for samples of noncritical compositions, while for samples with near-critical compositions the morphological evolution is responsible for the viscoelastic changes. Time-dependent experiments provide important information about morphological evolution at different temperatures. The region where fluctuations play a dominant effect on G' can be discerned from our treatment of putting G' and $\{G'(\omega)/[G''^2(\omega)T]\}^{2/3}$ in the same reference frame. On the basis of the results from both heating and cooling processes, it seems that there also exist competition between fluctuations and interfacial gradient on the determination of the value of G'.

Introduction

Phase separations in polymer systems were extensively investigated during the past 40 years both theoretically and experimentally.[1−10] Phase separation kinetics in the unstable region, which is also called spinodal decomposition, is fairly well understood.[5−10] However, recent developments show that the nucleation process in polymer phase transitions[11−15] may be more complicated than the traditional theoretical description,[16] which is suitable for most first-order phase transitions of one-component systems. Wang et al.[17,18] pointed out that fluctuation corrections to the mean field theory for polymer blends would bring out the metastable limit naturally. Balsara's experiment[11,12] showed that there is no natural difference between metastable region and spinodal region, implying that the nuclei are created by fluctuations, and their structures are diffusing and self-similar. The research[13] of Han et al. about simultaneously happened liquid−liquid phase separation and crystallization also suggested that the crossover of order parameters from one phase transformation to another may be possible. Like the study on nucleation and growth in metastable region, phase transitions in nonequilibrium state still remained as a largely unexplored area waiting to be studied. Phase separations under shear field are of both theoretical and practical importance. With respect to polymer blends, both shear induced mixing and shear induced demixing have been reported before.[19,20] Using time-resolved light scattering and neutron scattering, Han, Hashimoto, and Higgins et al.[19−21] have devoted lots of efforts in experimental studies and with many exciting results, which can be interpreted by theories developed by Onuki and Kawasaki.[22−24] But there are still many important questions yet to be answered.[25]

At the same time rheological measurements are often being used to study these processes and also have made many important advancements.[26−34] Taking advantage of rheology, these results are of crucial importance as applications are concerned. On one side, the phase-separated structures like droplet-matrix structure and bicontinuous structure in polymer blends can be reflected by rheological responses through the frequency dependence of storage modulus G'.[33−37] The interfacial tension of the dispersed phase prolong the whole relaxation spectra of the blend and results in a slowing down in the relaxation processes. Expressions have already been obtained to describe the behavior of droplet-matrix morphology in whole frequency space, while the situation is not so fortunate for the bicontinuous structure. On the other side, the fluctuations near the critical point of a blend, where the mass fluctuation is accomplished through the reptation of molecular chain, induce extra shear stress and hence elevate the storage modulus G' and the loss modulus G'' to a large extent. Ajji and Choplin were the first ones to deduce expressions[38] to evaluate the fluctuation effect on storage and loss modulus in homopolymer blends. Experimentally, Vlassopoulos, Madbouly, and Wang et al.[26−29] also extended this analysis to the off-critical components, and they believe that there also exists a fluctuation dominant region in metastable state. But until now researchers[26,27,29,33] are arguing about which factor, interface or fluctuation, dominates in the phase separation process both near and away from the critical point. However, it still seems to be an important success for both theorists and experimentalists who worked on this rheological problem in the past 20 years.

In this paper we take the advantage of our knowledge on shear-induced mixing,[19−21] newly discovered nucleation mechanism,[11,12] and the Ajji and Choplin treatments[38] to analyze the

* To whom all correspondence should be addressed: e-mail xiadong@iccas.ac.cn, c.c.han@iccas.ac.cn; Tel +86-10-82618089; Fax +86-10-62521519.
[†] Chinese Academy of Sciences.
[‡] Graduate School of the Chinese Academy of Sciences.
[§] Zhengzhou University of Light Industry.

10.1021/ma800646s CCC: $40.75
Published on Web 08/28/2008

origin of rheological behavior in the temperature ramp test and the nucleation phase separation kinetics.

Theoretical Background

The determination of binodal and spinodal points by rheology is widely used. We will summarize some of the previous techniques which have been used in the detection of the phase diagram. The temperature sweep or ramp process with fixed frequency and strain amplitude[26−29] is normally used to measure the binodal temperature. The point at which the storage modulus G' starts to increase (for low critical solution temperature systems) is usually defined as the binodal point. Thus, the time−temperature superposition principle (TTS) loses its correctness at this point. In the metastable region the nucleation phase separation process will create tiny dispersed regions in the matrix and introduce such a local concentration increase. But the detection of dispersed phase only occurs in enough quench depth of metastable region, and the hysteresis of upturn in G' is inevitable.[28] Besides, what we should keep in mind is that the growing concentration fluctuation in metastable region may elevate G', too.[39] Because of this there is no strictly defined formula for the nucleation theory, and we could not qualitatively calculate where the "real" binodal point is and the frequently used TTS method may not be so accurate. On the other hand, for near-critical composition, the basis of the upturning G' is attributed to the large fluctuation in the metastable region or near critical region, which results in excess stress.

The determination of spinodal point is a little bit complicated and not so straightforward. Ajji and Choplin used the mean field method[38] in analyzing G' and G'' which is frequently used to estimate the spinodal temperature. In turn, this is developed following Fredrickson and Larson's treatment[39]of order−disorder transition in block copolymers. Here we will briefly review their work and together with some of our considerations. Fredrickson and Larson established the relationship between the Fourier space vector and storage modulus G' and loss modulus G'' under the mean field condition by integrating through the whole space:

$$G'(\omega) = \frac{k_B T \omega^2}{15\pi^2} \int_0^{k_c} \frac{k^6 S_0^{\,2}(k)}{\omega^2 4\varpi^{-2}(k)} \left[\frac{\partial S_0^{\,-1}(k)}{\partial(k^2)}\right]^2 \mathrm{d}k \quad (1)$$

$$G''(\omega) = \frac{2k_B T \omega}{15\pi^2} \int_0^{k_c} \frac{k^6 S_0^{\,2}(k)\varpi(k)}{\omega^2 4\varpi^{-2}(k)} \left[\frac{\partial S_0^{\,-1}(k)}{\partial(k^2)}\right]^2 \mathrm{d}k \quad (2)$$

where $\varpi(k) = k^2 S_0^{\,-1}(k)\lambda(k)$, $S_0(k)$ is the static structure factor, $\lambda(k)$ is the Onsager coefficient, and k is the wave vector. These equations are suitable for both block copolymers and binary homopolymer blends. Then they take de Gennes' expression for static structure[1] factor under random phase approximation and neglecting higher order terms

$$S_0^{\,-1}(k) = 2(\chi_s - \chi) + \left[\frac{1}{\phi N_1}\frac{R_{g1}^{\,2}}{3} + \frac{1}{(1-\phi)N_2}\frac{R_{g2}^{\,2}}{3}\right]k^2 \quad (3)$$

where χ_s designates the interaction parameter in the spinodal point, χ is the interaction parameter, R_{gi} denotes the radius of gyration of species i, and N_i is the number of statistical segments. With the expression for the Onsager coefficient described by Binder,[3] then

$$\lambda^{-1}(k) = \frac{1}{\phi a_1^{\,2} W_1} + \frac{1}{(1-\phi)a_2^{\,2} W_2} + \left[\frac{R_{g1}^{\,2}}{\phi a_1 W_1} + \frac{R_{g2}^{\,2}}{(1-\phi)a_2 W_2}\right]k^2 \quad (4)$$

where a_i is the statistical segment length of repeated unit for species i and W_i its rate of reorientation, with definition

$$W_i = 3\pi k_B T/\zeta_i \quad (5)$$

with ζ_i the monomeric friction coefficient. Finally, they obtained the G' and G'' expressions for the terminal flow region near the critical point

$$G'(\omega) = \frac{k_B T \omega^2}{1920\pi}\left[\frac{1}{3}\left\{\frac{R_{g1}^{\,2}}{\phi N_1} + \frac{R_{g2}^{\,2}}{(1-\phi)N_2}\right\}\right]^{1/2}\left[\frac{1}{\phi a_1^{\,2} W_1} + \frac{1}{(1-\phi)a_2^{\,2} W_2}\right]^2 [2(\chi_s - \chi)]^{-5/2} \quad (6)$$

$$G''(\omega) = \frac{k_B T \omega}{240\pi}\left[\frac{1}{3}\left\{\frac{R_{g1}^{\,2}}{\phi N_1} + \frac{R_{g2}^{\,2}}{(1-\phi)N_2}\right\}\right]^{-1/2}\left[\frac{1}{\phi a_1^{\,2} W_1} + \frac{1}{(1-\phi)a_2^{\,2} W_2}\right][2(\chi_s - \chi)]^{-1/2} \quad (7)$$

From the above calculation, they concluded that G' is more sensitive to temperature than G'' if simply writing χ as $\chi = A + B/T$. They also found something interesting when calculating the ratio $G'(\omega)/G''^2(\omega)$ by substituting R_{gi} to be $R_{gi} = N_i a_i^{\,2}/6$

$$\frac{G'(\omega)}{G''^2(\omega)} = \frac{30\pi}{k_B T}\left\{\frac{a_1^{\,2}}{36\phi} + \frac{a_2^{\,2}}{36(1-\phi)}\right\}(\chi_s - \chi)^{-3/2} \quad (8)$$

Since the correlation length in polymer blend can be expressed by

$$\xi = \frac{a'}{6}\{\phi(1-\phi)(\chi_s - \chi)\}^{-1/2} \quad (9)$$

where a' is the characteristic length which related to individual unit length a_i as

$$\frac{a'^{\,2}}{\phi(1-\phi)} = \frac{a_1^{\,2}}{\phi} + \frac{a_2^{\,2}}{1-\phi} \quad (10)$$

so the final expression of the ratio could connect to the correlation length through

$$\frac{G'}{G''^2} = \frac{30\pi}{k_B T}\xi^3 \quad (11)$$

But one of the restrictions of these equations is that the sample must near the critical point to achieve large enough correlation length. Assuming a simple form of χ to be $\chi = A + B/T$,[26] a linear relation could be obtained through $\{G''^2(\omega)/[G'(\omega)T]\}^{2/3}$ vs $1/T$, which lead to an intercept at $1/T$ axis denoting the spinodal temperature, T_s. Thus, we could finally obtain the spinodal point through temperature ramp test under low frequency.

The interfacial effect in a well phase separated polymer blend system is prominent. Rheological treatments were independently developed by Palierne, Bousmina, and Lee et al.,[40−43] in which the calculations have been proven to be quite good and useful.[44,45] Here we take the most widely used Palierne model as an example to analyze our dispersed system. If we assume that the interfacial tension and the variation of interfacial is independent of local shear at low frequency, which also means that there is no shear induced mixing, a simplified version for complex modulus[41,44] could be obtained as

$$G'_{\mathrm{blend}} = (\phi_A G'_A + \phi_B G'_B) + \frac{\omega^2 \eta_0(\tau_1 - \tau_2)}{1 + \omega^2 \tau_1^{\,2}} \quad (12)$$

$$G''_{\mathrm{blend}} = (\phi_A G''_A + \phi_B G''_B) + \frac{\omega^2 \eta_0(1 + \omega^2 \tau_1 \tau_2)}{1 + \omega^2 \tau_1^{\,2}} \quad (13)$$

where ϕ_A and ϕ_B are volume fraction of components A and B. η_0 is the zero-shear viscosity of the blend mixture, and τ_1 is the

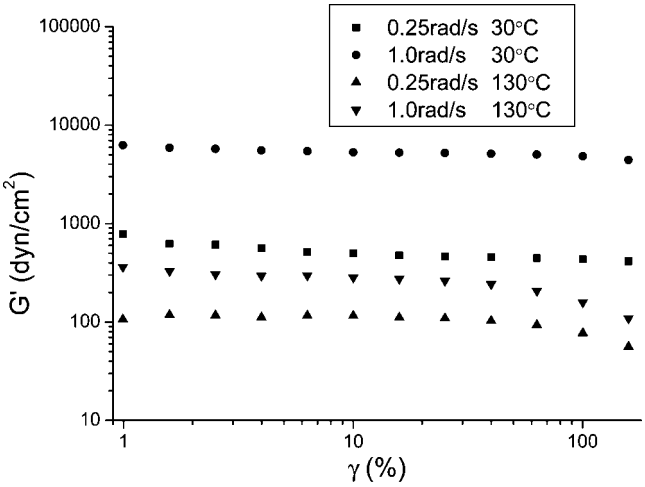

Figure 1. Strain dependence of the storage modulus of LPI80 is shown, with frequencies of 0.25 and 1.0 rad/s at 30 and 130 °C, respectively.

longest relaxation time while τ_2 is a retardation time and expressed as

$$\eta_0 = \eta_m \frac{10(\lambda+1)+3\phi(5\lambda+2)}{10(\lambda+1)-2\phi(5\lambda+2)} \quad (14)$$

$$\tau_1 = \frac{R\eta_m}{4\sigma}\frac{(19\lambda+16)[2\lambda+3-2\phi(\lambda-1)]}{10(\lambda+1)-2\phi(5\lambda+2)} \quad (15)$$

$$\tau_2 = \frac{R\eta_m}{4\sigma}\frac{(19\lambda+16)[2\lambda+3-3\phi(\lambda-1)]}{10(\lambda+1)+3\phi(5\lambda+2)} \quad (16)$$

where $\lambda = \eta_d/\eta_m$ is the ratio of viscosity between dispersed phase and matrix phase, ϕ is the volume fraction of dispersed droplet phase, σ is the interfacial tension, and R is the averaged droplet radius. There is one crucial restriction on the morphology of our system when applying these expressions, that is, the radius distribution of the droplets cannot be too wide, i.e., more than 2.2.[41]

The first theory considers no interface effect while the second one does not introduce fluctuation effect. In other words, one is for a system undergoing with large concentration fluctuations, and the other is for a phase separated droplet−matrix system with defined interfaces. But the incorporation of both of these two analyses in the interpretation of rheological behavior is crucial. Because different phase conditions of polymer blends will determine which effect, fluctuation or interface, gives the main contribution to the viscoelastic behavior.

Experimental Section

Materials. The polymers used in this research were synthesized by Beijing Yanshan Petrochemical Co., Ltd. The two statistical polymers, polybutadiene (PB) and low vinyl content polyisoprene (LPI), were characterized by gel permeation chromatography (GPC), ^{2}H nuclear magnetic resonance (NMR), volume exclusion density measurement apparatus, and differential scanning calorimetry (DSC), and the detailed results are summarized in Table 1. Polymer blends were prepared by the solution blending method.[44] PB/LPI blend is labeled as LPI*x*, where *x* represents the weight fraction of LPI in the blend. For example, LPI80 means that LPI contained of the sample is 80 wt %. We started with a dilute solution (mass fraction of 2% of the total polymer), which contains the antioxidant butylated hydroxytoluene (BHT) with mass fraction 0.05% of the solution, in a solvent of methylene chloride.[44] Then the solution was filtered through a 1 μm Millipore filter, and the solvent was evaporated at 35 °C with stirring. Samples were further dried in vacuum oven at 15 °C for a week in order to remove the remaining methylene chloride.

Rheological Measurements. The viscoelastic properties of samples were obtained with an ARES rheometer. We chose the 25

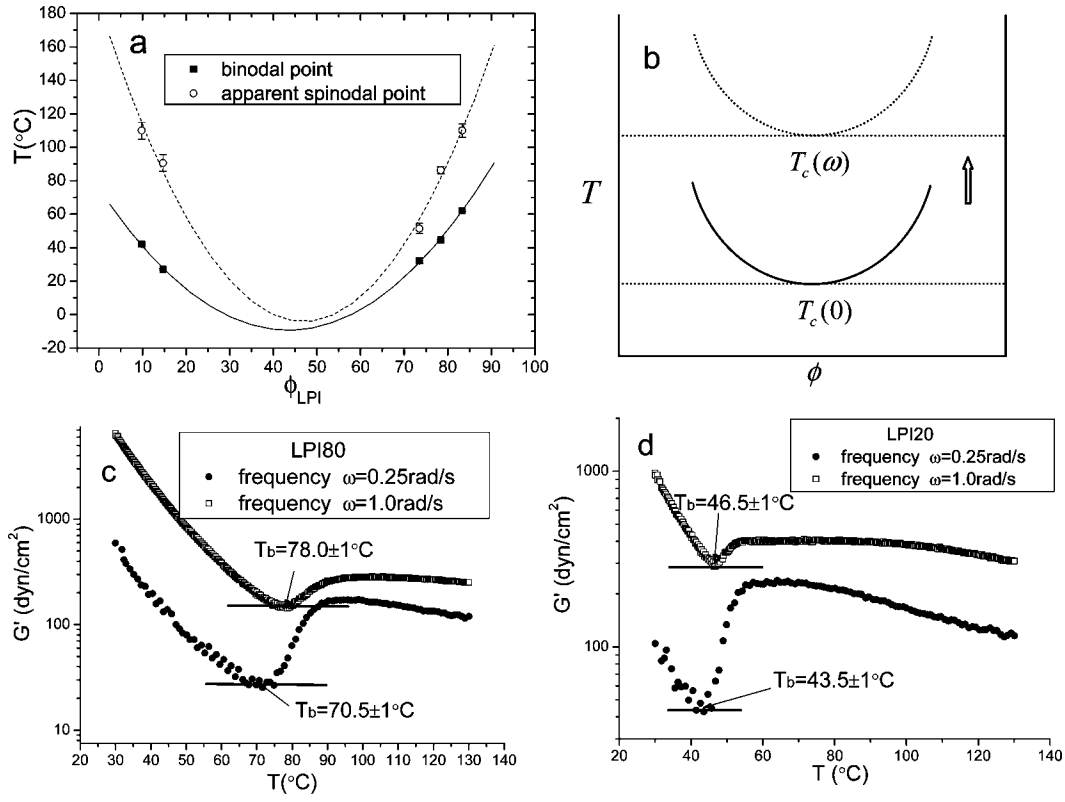

Figure 2. (a) Static LCST phase diagram of PB/LPI blend is estimated by a least-squares fitting of the experimental data. (b) Illustration of frequency dependence phase diagram. (c) Frequency dependence of the apparent binodal points of LPI80. (d) Frequency dependence of the apparent binodal points of LPI20.

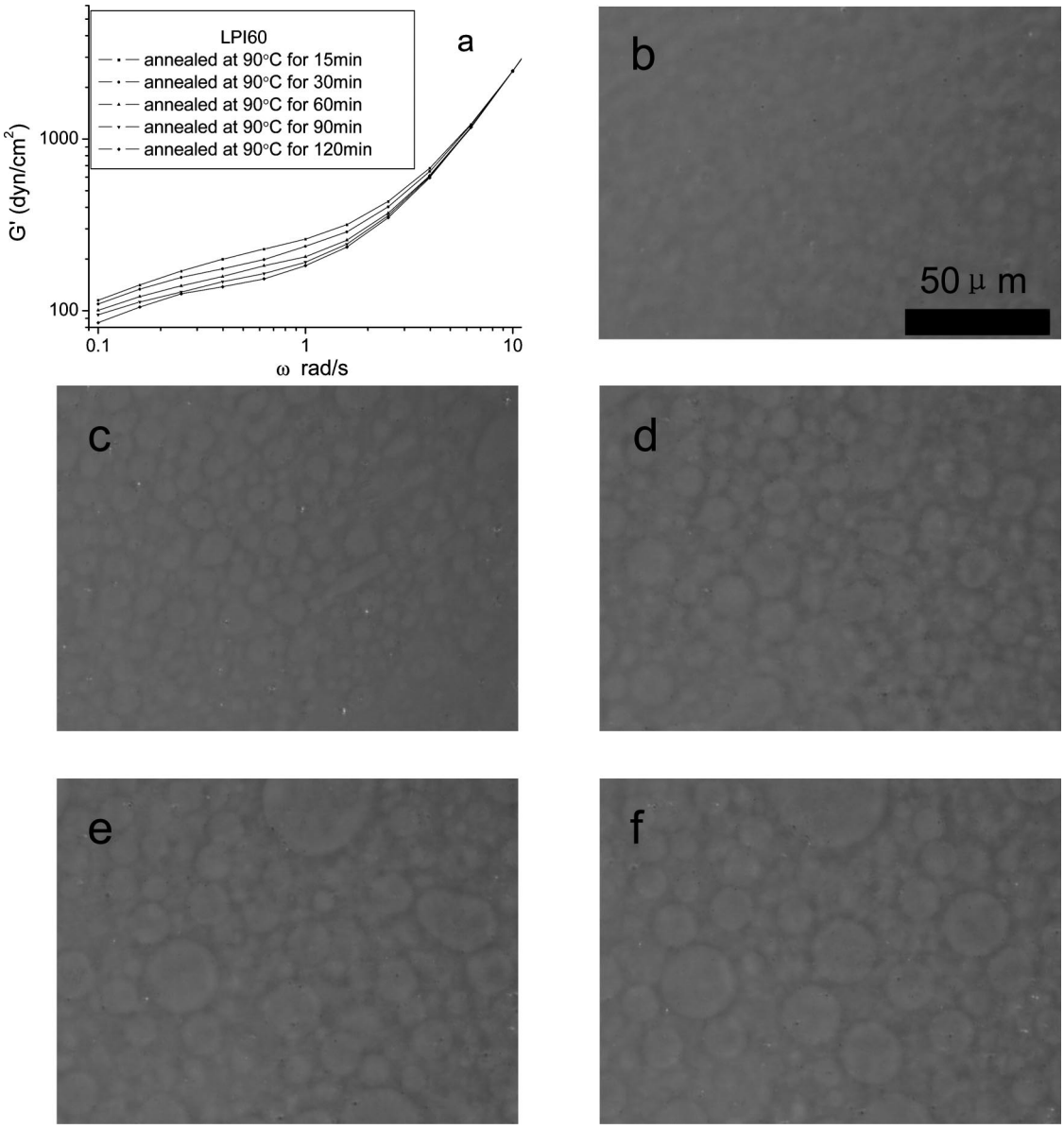

Figure 3. (a) Frequency dependence of the storage modulus G' of LPI60 with different annealing time at 90 °C. Photograph of typical droplet-matrix morphology for LPI60 after annealing at 90 °C for (b) 15, (c) 30, (d) 60, (e) 90, and (f) 120 min. The scale bar is the same for each photograph.

Table 1. Characterization Data of Polymers

sample code	M_n (g/mol)	M_w/M_n	density (g/cm^3)	T_g (°C)	microstructure, mol %		
					1,4-	1,2-	3,4-
PB	55 000	1.10	0.877	−97	89	11	0
LPI	34 000	1.50	0.895	−63	88	0	12

mm parallel plates with gap value of 500 μm to execute our measurements. All of our experiments were carried out under the protection of nitrogen to prevent degradation of thermal sensitive elastomers. All samples were kept at 4 °C in a refrigerator and then put into a vacuum oven at 20 °C for 2 days to remove air bubbles before experiment and to ensure the same thermal history. In temperature ramp and frequency sweep experiments the strain amplitude was set at 10% to make sure all experiments are carried out in the "apparent" linear viscoelastic region for each of the two sweeps. Actually, this "apparent" linear viscoelastic region is a steady state; just for convenience we used the language "apparent" linear region. This is related to the essential issues of this study which will be discussed through out the rest of this paper. The temperature ramp rate is 1 °C/min for most experiments and frequencies. The exception is LPI80 under 0.25 rad/s; we adopted a different ramp rate in some temperature region just for comparison. Temperature control in the rheometer is carried out by hot nitrogen gas with accuracy of ±0.1 °C. All the experiments started from 30 °C, at which temperature samples are already in the phase-separated region except LPI80. The maximum shear rate under oscillatory shear of 0.25 and 1 rad/s are not too big, and the values are 0.025 and 0.1 s^{-1}, respectively, which are not too large to cause excessive shear mixing.

Table 2. Average Radius of Droplet in LPI60 at 90.0 °C with Different Phase Separating Time

LPI60	15 min	30 min	60 min	90 min	120 min
number-average radius R_n (μm)[a]	5.3	7.7	10.1	11.8	12.6
volume-average radius R_v (μm)[a]	6.7	9.9	13.4	17.5	19.6
R_v/R_n	1.26	1.29	1.33	1.48	1.56

[a] The average radius of dispersed droplet is obtained by averaging at least 80 droplets in the photograph.

Optical Microscopy (OM). The phase contrast optical microscope (PCOM) observations were carried out using an Olympus (BX51) optical microscope and Olympus (C-5050ZOOM) camera.

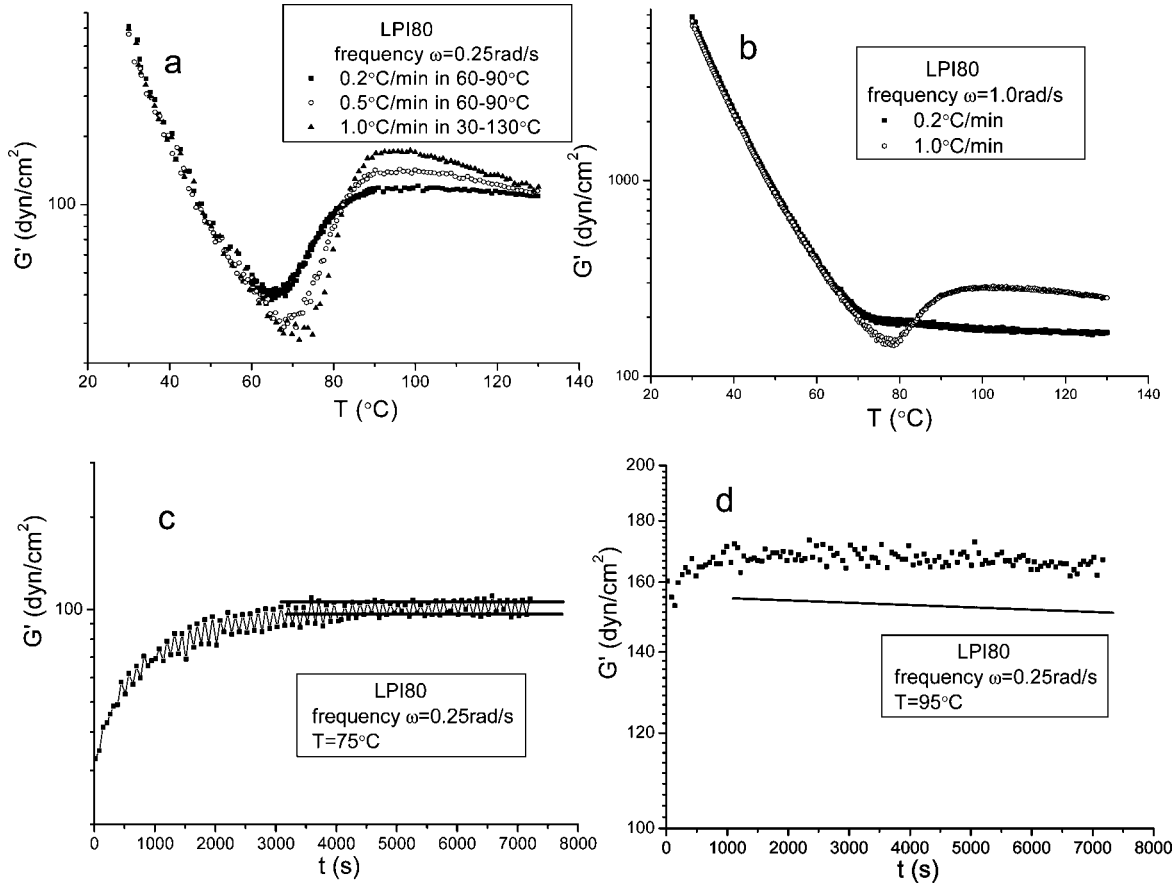

Figure 4. Temperature ramp test results of G' with strain of 10% for LPI80 under frequencies of (a) 0.25 rad/s and (b) 1.0 rad/s, during which the ramp rate is varied. The time dependence of the storage modulus G' of LPI80 when achieved at (c) 75 °C and (d) 95 °C with frequency of 0.25 rad/s and strain of 10%. Level lines are only the guides for the eyes.

The experimental temperature was controlled by a Linkam (LTS 350) hot stage. Samples were kept between clean microscope slides and cover glass with about 30 μm in thickness. Samples were first phase separated into large domains as temperature increased, and then the temperature was lowered to find out at which temperature we could bring the sample back into homogeneous states. This binary search process is repeated until the binodal point is fixed.

Results and Discussion

The Steady State Region. The advantage of keeping the experiment in the steady state is to simplify our data analysis and discussion and also to make contact with reported literature results. In our frequency or temperature sweep tests, we used small strain amplitude of 10% to keep all the experiments in the steady state region. In this region, the modulus changes with time only in the temperature sweep whenever the process of shear mixing happens, but for constant temperature and the time scale in our study the modulus remains nearly constant. We show in Figure 1 the LPI80 strain sweep experimental results to illustrate this.

Shear Induced Mixing Effect. Although there is a well-defined theory for the phenomenon of shear induced mixing under steady shear flow or so-called simple shear flow,[22−24] interpretations for such a phenomenon under oscillatory shear are not available. So we just used our basic knowledge under steady shear and make an analogy between steady shear and oscillatory shear. The theory of MCRG[22−24] (mode coupling renormalization group) is often used to interpret the shear induced mixing phenomenon. The origin of the shear induced mixing phenomenon can be understood intuitively regardless of the underlying complicated physics. For a shear rate $\dot{\gamma}$, fluctuations with relaxation time slower than $\dot{\gamma}^{-1}$ are distorted, then the shear induced mixing phenomenon happens naturally. Similar systems to what we used here have been studied before, and the phenomenon of shear induced mixing took place under steady shear flow.[46,47] The static binodal points of Figure 2a are obtained with optical microscopy with procedures explained in the previous section of Optical Microscopy. The apparent "spinodal points" are extrapolated by a frequency-dependent method as will be discussed below. The binodal line and the apparent "spinodal line" are all obtained by polynomial fit to guide the eye. The effect of oscillatory shear can also suppress the fluctuations and shift the apparent phase separation temperature or delay the phase separation process in a temperature sweep experiment. The influence of oscillatory shear on phase diagram is illustrated in Figure 2b. Figure 2c shows three LPI80 temperature ramp experiments with two different frequencies, where the ramp rate is fixed on 1.0 °C/min, and we define the point where the differential of G' on T equals 0 as the apparent binodal point. The promoted cloud points under frequencies 0.25 and 1 rad/s correspond to 70.5 ± 1 and 78.0 ± 1 °C, respectively. Compared to the static binodal point of 44.5 °C in Figure 2a, it is clear that under the oscillatory shear the cloud point changed a lot. Figure 2d shows the elevated cloud points of LPI20 under frequency 0.25 and 1 rad/s; the corresponding temperatures are 43.5 ± 1 and 46.5 ± 1 °C, respectively, compared to the quiescent cloud point (extrapolated) from Figure 2a of below 20 °C. But in samples LPI40 and LPI60, which will be discussed later, we could not obtain any clear shear induced binodal point with the low frequencies we have used.

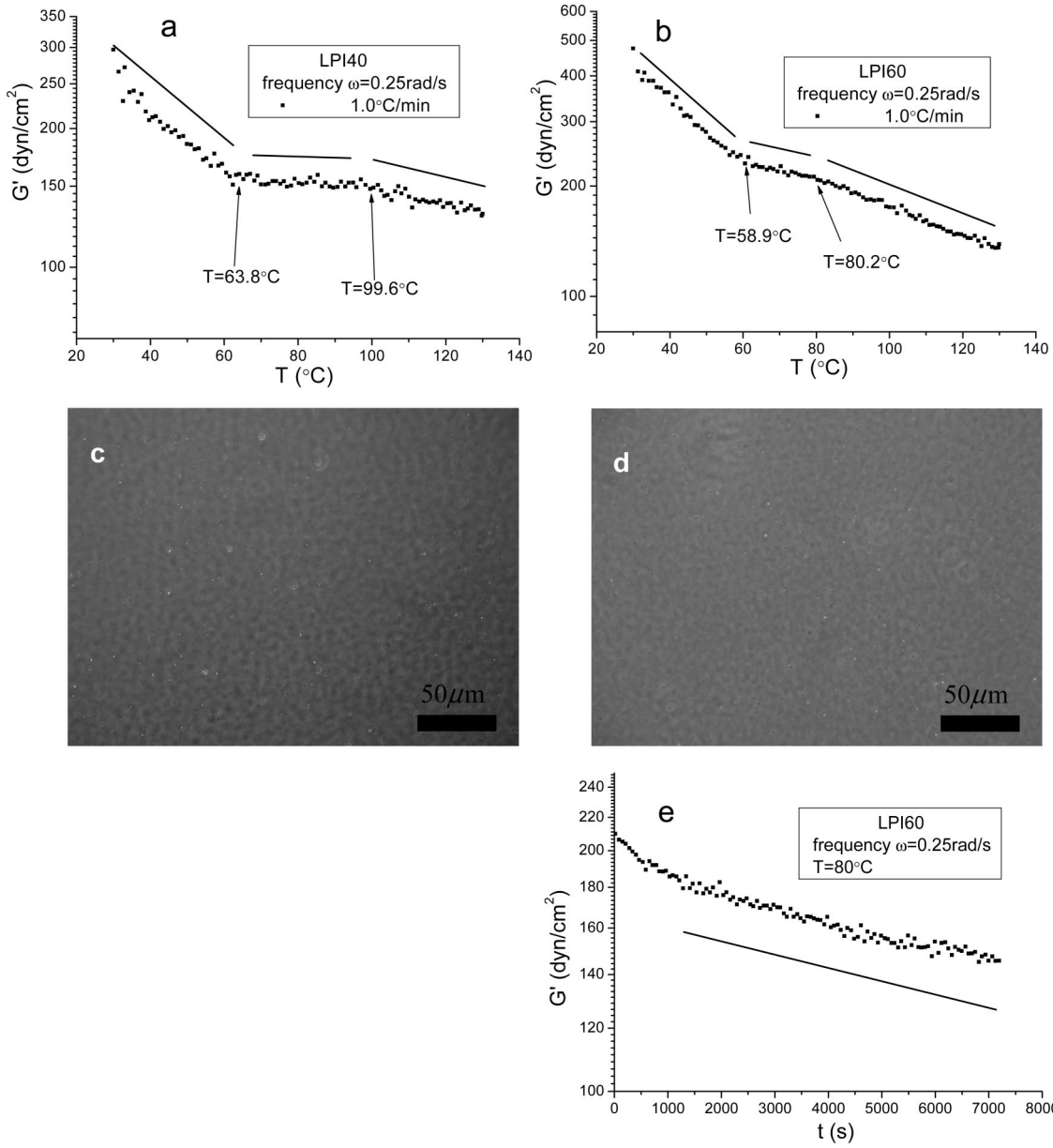

Figure 5. Temperature dependence of G' with frequency of 0.25 rad/s, strain 10%, and ramp rate of 1.0 °C/min for (a) LPI40 and (b) LPI60. The circled temperature is the location of time sweep experiments, and linear lines are indications of the linear part in G'; a typical bicontinuous structure is shown in (c) LPI40 and (d) LPI60. (e) Time dependence of G' of LPI60 with frequency of 0.25 rad/s and strain of 10% at 80 °C. Lines are only guides for the eyes.

Their temperature ramp curves in Figure 5 do not show any rapid upturn, indicating that large phase separated structures have already formed and the blend has lost the ability to form structures through the nucleation−growth process.

Analysis of the Storage Modulus in a Temperature Ramping Process and the Corresponding Phase Separation Mechanism. In the heating process, the slightly phase separated LPI20 and homogeneous LPI80 show similar viscoelastic behavior as illustrated in Figure 2c,d. Slightly phase separation in LPI20 did not change the local concentration too much, and it still has the ability to nucleate in the metastable region under shear. These two samples hold a similar nucleation process which will be discussed later again and naturally gives a similar rheological response. The quantitative difference between G's with different ramp rates can be interpreted by the following mechanism.

The storage modulus G' will change while increasing the dimension of dispersed phases in the intermediate frequency region, 0.1−1 rad/s. This result is shown in Bousmina's numerical analysis on Palierne model with changing the ratio of R/σ without any experimental basis.[48] Here we fix all of the parameters except the droplet dimension R and let

$$C_1 = \frac{\eta_m}{4\sigma}\frac{(19\lambda+16)[2\lambda+3-2\phi(\lambda-1)]}{10(\lambda+1)-2\phi(5\lambda+2)} \tag{17}$$

$$C_2 = \frac{\eta_m}{4\sigma}\frac{(19\lambda+16)[2\lambda+3-3\phi(\lambda-1)]}{10(\lambda+1)+3\phi(5\lambda+2)} \tag{18}$$

Then the derivatives of G' and G'' with R are expressed as

$$\frac{\partial G'_{\text{blend}}}{\partial R} = -(C_1-C_2)\omega^2\eta_0\frac{1}{\left(\frac{1}{C_1R}+C_1\omega^2R\right)^2}\left(\omega^2-\frac{1}{{C_1}^2R^2}\right) \tag{19}$$

$$\frac{\partial G''_{\text{blend}}}{\partial R} = -4{C_1}^3C_2\omega^6\eta_0\frac{R^2}{(1+\omega^2{C_1}^2R^2)^2} \tag{20}$$

It is obvious in eq 19 that there exist a critical radius $R_c = (C_1\omega)^{-1}$ for the storage modulus G'. Below this critical dimension G' will increase with the increasing of the droplet

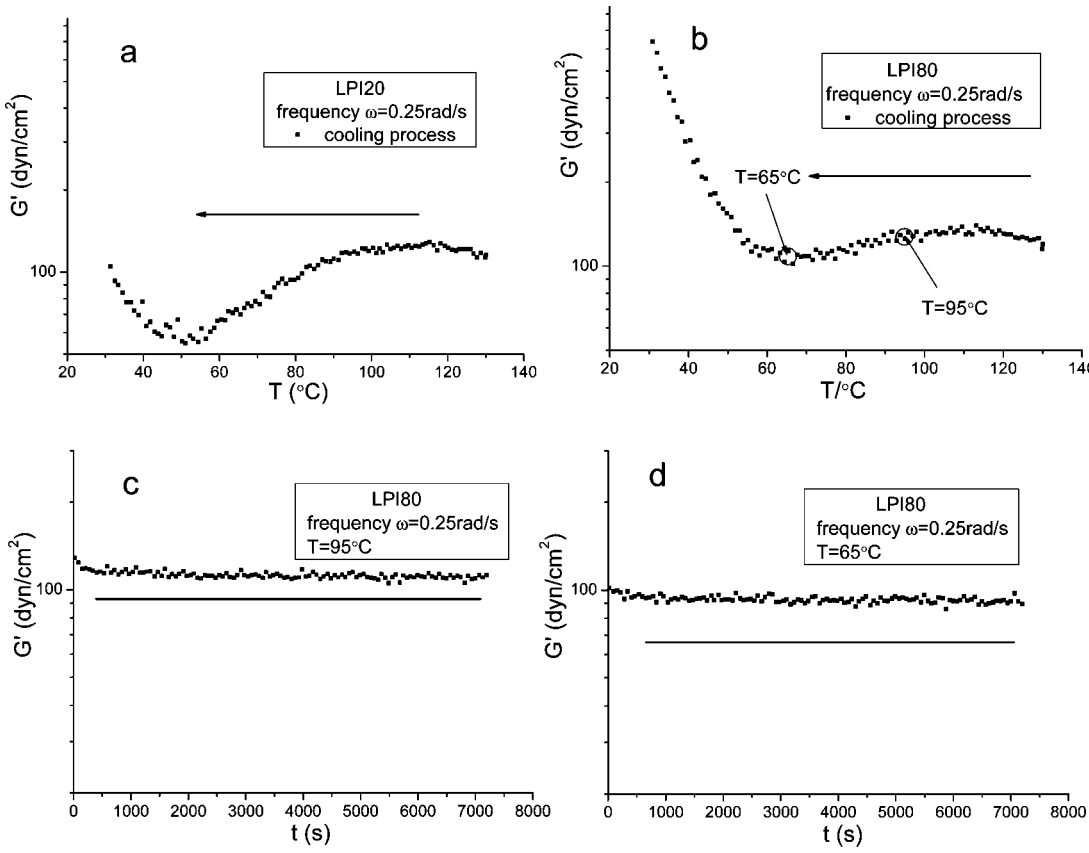

Figure 6. Temperature dependence of the storage modulus G' in cooling process with frequency of 0.25 rad/s, strain of 10%, and ramp rate of 1.0 °C/min for (a) LPI20 and (b) LPI80 and the corresponding time dependence experiment at the circled temperature with the frequency of 0.25 rad/s and strain of 10% for LPI80 at (c) 95 °C and (d) 65 °C. Level lines are only guides for the eyes while arrows are the indication of cooling process.

radius R while above this value G' will decrease with the increasing R. But the loss modulus G'' will always decrease with the increasing R. Here we did a numerical calculation on the sample LPI60, assuming that the interfacial tension remains constant at high temperatures during the late stage of phase separation.[44] The unknown interfacial tension is estimated to be around the order of 1 mN/m;[44] the matrix viscosity η_m is approximated by the pure LPI, 705 Pa·s; the droplet viscosity is substituted by that of pure PB, 673 Pa·s; and the dispersed phase with volume fraction ϕ_d as 0.406; all these data except volume fraction are at 90 °C. Obviously such treatments are not suitable for nucleation process when the new phase volume fraction is continuously increasing. But once the dispersed volume is constant and the interface is well-defined, our analysis can be qualitatively correct. On the basis of these values, the relaxation time $\tau_1 = 2.117 \times 10^6 R(s)$ and the retarding time $\tau_2 = 1.076 \times 10^6 R(s)$ are obtained as functions of droplet dimension R. The critical radius R_c is $4.724 \times 10^{-7}\omega^{-1}(m)$. The storage modulus of homogeneous components in high-frequency region (10−100 rad/s) is very large, where the interfacial tension does not contribute too much to its value. On the contrary, in the low frequency region (0.1−1 rad/s), the storage modulus is controlled mainly by the interfacial tension. Under the frequency of 0.25 rad/s, the critical dimension of R_c is about 2 μm.

We placed the sample LPI60 under 90 °C, deep enough quench to eliminate the effect of volume fraction change for different times, and then executed the frequency sweep measurements. Figure 3a illustrates the difference of frequency sweep curves with different annealing time at 90 °C. The "shoulder" value of G' in the 0.1−1 rad/s region decreases with the phase separating time. The microscopy graph in Figure 3 clearly shows that the dimension scale of droplets grow with the phase separating time. The average radius of droplet in Table 2 shows that the dimension of the dispersed phases is already larger than the estimated R_c after phase separating for 15 min at 90 °C. Thus, the results in Figure 3a only exhibit the decreasing effect of droplets dimensions (increasing) on G'. The single positive effect of radius of droplet is not observed in this case. However in the case of Vinkier et al.,[33] they have provided a positive slope affected by both volume fraction of dispersed phase and the radius of droplets in binodal region. The increasing of dispersed phase volume or, in other words, the increasing number of droplets provides more interfaces, which will certainly prolong the relaxation time of polymer blend and promote the storage modulus. These two factors are related to two different kinetic processes, and we will pay more attention to this in the following discussion.

In metastable region, kinetic competitions for structures formation also existed, which will in turn affect the viscoelastic properties. According to the newly published results,[11−13] the nuclei are not solids with sharp interface, also they do not have regular shape as described by traditional theory described.[16] They are maybe just tiny regions with diffused boundaries and irregular shapes;[11−13] as a result, the effect of such interfaces which affect the rheological behavior must follow the appearance of unambiguous interface structures. On the basis of the above discussion, the formation of droplet must have two steps of kinetic processes. The formation of nuclei and the growth of a droplet with a clear defined interfacial structure. Thus, the two kinetic processes will affect each other in the whole metastable region as long as the blend has strong enough fluctuations to continuously bring out the nuclei. Our experimental work can be interpreted very well by this nucleation

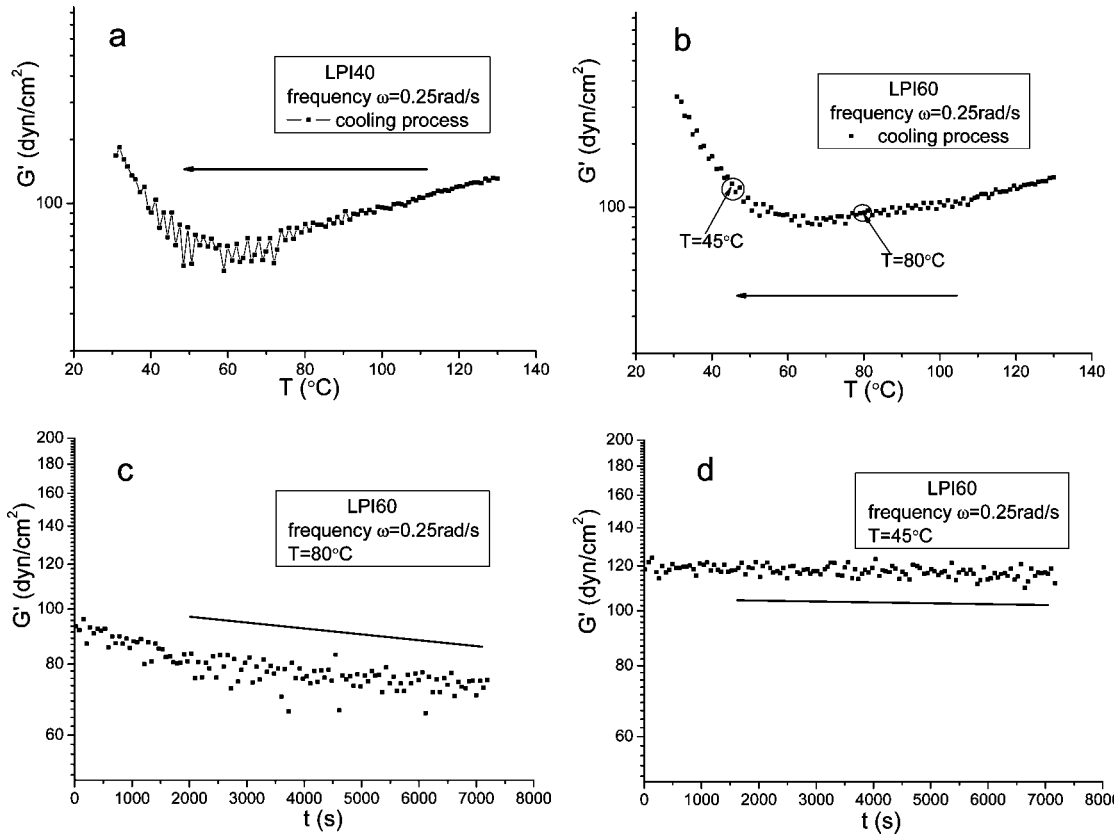

Figure 7. Temperature dependence of the storage modulus G' in cooling process with frequency of 0.25 rad/s, strain of 10%, and ramp rate of 1.0 °C/min for (a) LPI40 and (b) LPI60 and the corresponding time-dependent experiment at the circled temperature point with the frequency of 0.25 rad/s and strain of 10% for LPI60 at (c) 80 °C and (d) 45 °C. Lines are only guides for the eyes while arrows are the indication of cooling process.

and growth mechanism. We vary the temperature ramp rates to 0.2, 0.5, and 1.0 °C/min with a fixed frequency of 0.25 rad/s in the temperature range of 60−90 °C for LPI80 as shown in Figure 4a; the heating rate is 1.0 °C/min for the remaining parts of all experiments. This procedure changes the time scale while passing through the metastable region for LPI80. It is obvious in Figure 4a that the resulting differences on storage modulus are prominent. The discrepancy of obtained binodal points in these three experiments can also be found elsewhere[28] and was interpreted by the slow kinetics of nucleation compared with temperature ramp rate. Then the maximum of G' is reached near 90 °C independent of the heating rate, which means that the nucleation−growth kinetics was ceased and replaced by the spinodal decomposition kinetics if the phase separation has not reached its coexistence compositions yet. The maxima of G' are very different in their height, which can be attributed to the different average size of droplets. If we reduce the speed while passing through the metastable region more nuclei will be formed, but at the same time the growth of these tiny droplets will also gain more duration. It is believed in our case that at the end of binodal region the droplet size is much larger than R_c, and the negative effect of large droplet dimension on G' is more prominent than the positive effect of the number of droplets on G'. Eventually the effect of droplet growth on G' wins in the competition with nucleation. If the nucleation kinetic has more contribution than the growth, the result will be inversed. This is shown in Madbouly's work; the higher the temperature ramp rate, the lower the storage modulus G'.[28] Thus, we conclude that the kinetic competition between nucleation and nuclei growth determines whether the slowing down of temperature ramp rate will produce higher or lower maximum of G' before crossing into the unstable region. The viscoelastic evolution in the unstable region, where only dimension and constitution of droplets evolve, is totally different from the metastable one. We could observe the rapid decrease of the G' because of the rapid growth of droplets and nearly constant interfacial tension.[44] Figure 4b illustrate the LPI80 temperature ramp experimental results from two different ramp rates under the frequency of 1 rad/s, and it shows a similar trend as in Figure 4a. The disappearance of upturn of G' in Figure 4b in the 0.2 °C/min ramp rate test may be caused by the large droplet size.

Time-dependent experiments of LPI80 are also carried out after temperature ramp to certain temperatures under frequency of 0.25 rad/s. Figure 4c,d shows the kinetics of phase separation at different phase conditions. Because of the nucleation in the metastable region at 75 °C, the storage modulus increases rapidly, and it was stabilized after more than 1 h. Then the interesting wavelike oscillation of G' continued as is shown in Figure 4c. In other experimental measurements, such a synchronized phenomenon was not observed, except in the temperature dependence experiment in Figure 7a which shows similar results. We are sure that this phenomenon is not introduced by the systematical error of our instrument and is probably caused by the coupling of the droplet shape change period (relaxation time) with the periodical measurements, and further investigation is definitely needed in the future. At 95 °C in Figure 4d the time-dependent result only shows a little increase in the first 10 min and then become nearly stable. Such weak increase may be due to the increase of interfacial tension as the component in dispersed phase changes, and the system should be into the unstable region already.

Unfortunately, for samples LPI40 and LPI60 there are no obvious nucleation characteristics from the temperature ramp curves, as shown in Figure 5a,b. The shear effect due to our low-frequency shear is probably not so significant in these deep phase separation cases. In Figure 5c,d, we can clearly see that

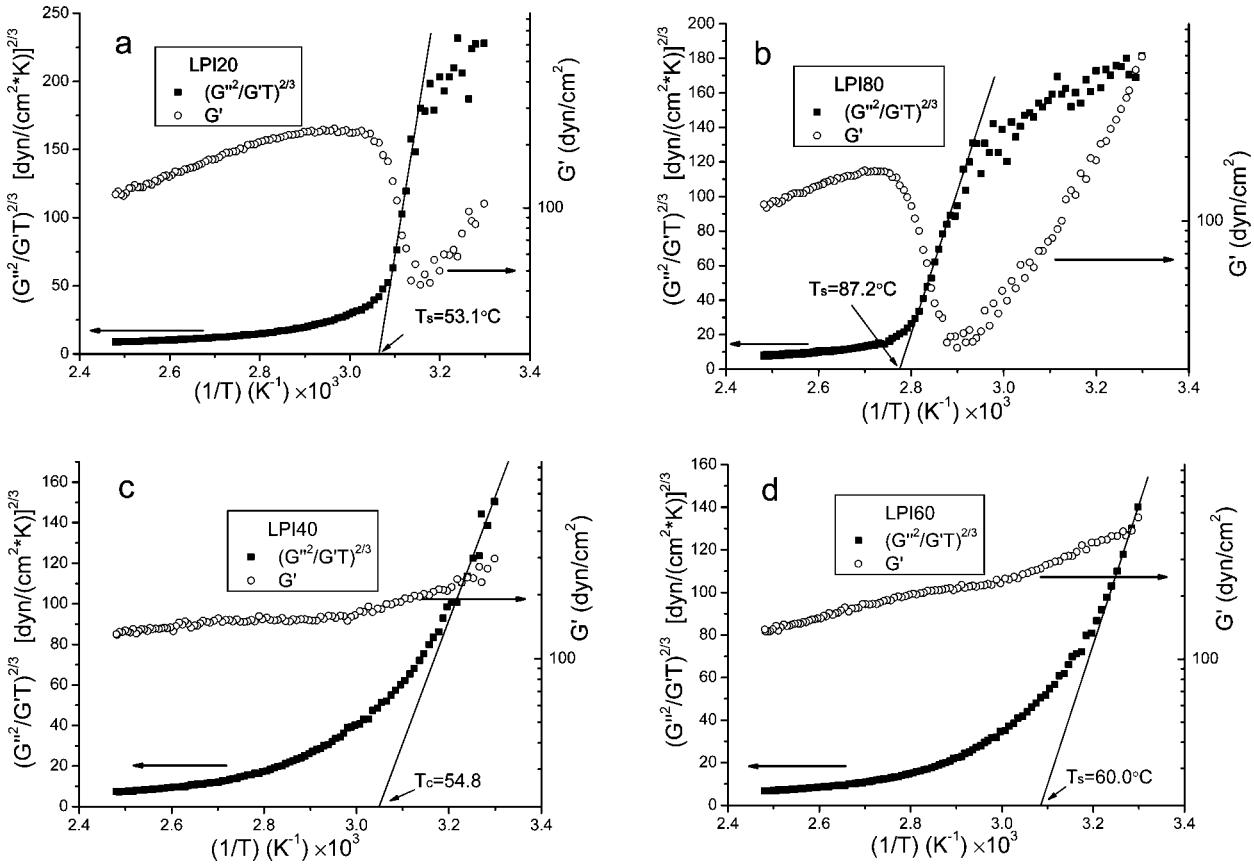

Figure 8. Storage modulus G' and the corresponding calculated value of $(G''^2/G'T)^{2/3}$ in heating processes vs $1/T \times 1000$ of (a) LPI20, (b) LPI80, (c) LPI40, and (d) LPI60.

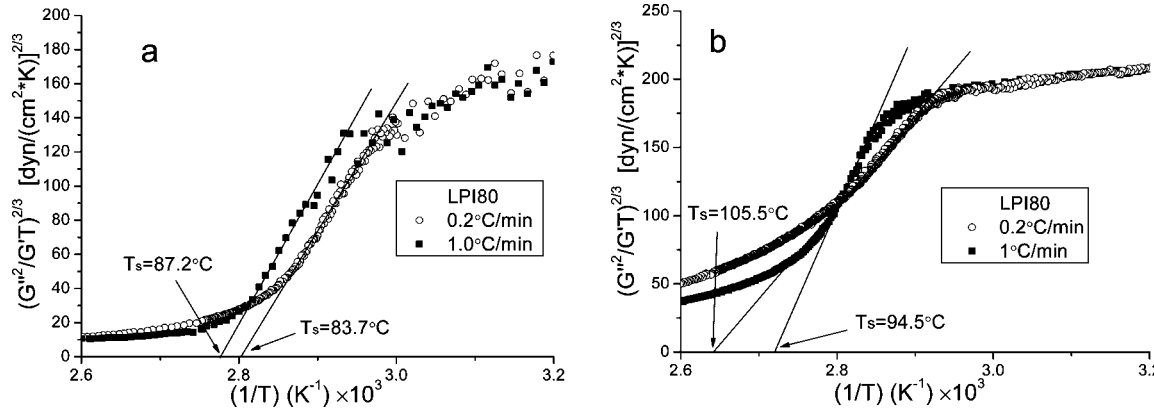

Figure 9. Plots of $(G''^2/G'T)^{2/3}$ vs $1/T \times 1000$ of LPI80 in heating processes with different ramp rates of 0.2 and 1.0 °C/min under frequencies of (a) 0.25 rad/s and (b) 1.0 rad/s.

the bicontinuous structures have already existed in the two samples after the treatment of removing the air bubble in vacuum. The nucleation ability is eliminated by the fact that these samples are already into the unstable region and bicontinuous structures have already formed. Three linear regions of storage modulus can be distinguished under the temperature ramp test at 0.25 rad/s, which may be related to the morphological evolution from bicontinuous to droplet-matrix structure. Such a kind of conclusion needs more support from microscopic results, which we will try in the future. Figure 5e shows the time sweep result of LPI60 at 80 °C. The storage modulus G' was continuously decreasing for 2 h, which was obviously due to a continuous morphological evolution. The only thing we can speculate at this time is that the bicontinuous structures have went through a coarsening and breakup stage (the second linear region), and continuous coalescence and growth of droplets can only led to a reduction of interfacial contribution to the measured G'. This explanation is consisted with the third linear stages in both Figure 5a and Figure 5b and also with the time dependence of data shown in Figure 5e.

Viscoelastic Response in Cooling Process. In the cooling curves for LPI20 and LPI80 in Figure 6a,b, G' decreased a lot due to the melting of droplets and consequently the decreasing of interfacial tension. But we must also note that at high temperatures around 110 °C the storage modulus even increased somewhat, and the reason is unknown. One possibility is that during the melting process small structures melt first and large structures melt slowly.[49] The change of discrete size distribution could cause some transient effect on G'. The time sweep experiments of LPI80 at 95 and 65 °C during the ramping down process in Figure 6c,d show that the morphological evolution

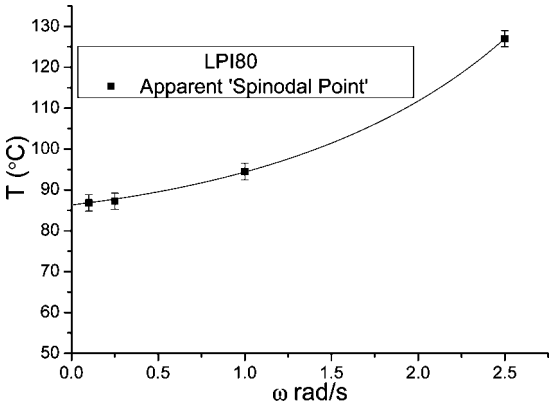

Figure 10. Frequency-dependent on apparent "spinodal point" of LPI80 with the temperature ramp rate at 1 °C/min.

of off-critical component is very slow. Droplet dimensions were kept nearly constant in cooling process. For the cooling behavior in Figure 7a,b of the near-critical samples LPI40 and LPI60, we could not observe any increase of G' at high temperatures. Figure 7c,d shows time sweep characteristic of LPI60 at 80 and 45 °C. It is obvious that at 80 °C the size of dispersed phase is still increasing. While at 45 °C the shear induced mixing state may have already achieved, which will be shown in the following section. And the evolution of storage modulus only showed a small decrease with the dissolution of discrete domains, which means that the effect of the interface as well as the fluctuation effects are becoming weaker.[49]

Extrapolating to the "Spinodal Points" Figure 8a−d shows $(G''^2/G'T)^{2/3}$ vs $1000/T$ results for the four samples during their heating processes. We need to find the linear part of the plot in order to extrapolate to the "spinodal point". This method used expressions from Ajji and Choplin's analysis,[38] which was developed under the critical conditions. Once we used this kind of data treatment, it means that we have already used the hypothesis that the critical-like fluctuations appear near the spinodal line. On the other hand, according to Balsara's experiments,[11,12] there is no divergence of fluctuations while passing from metastable region into the spinodal region under quiescent condition. Here we have to assume that the nonequilibrium situation will show different phase separation mechanisms in metastable and unstable region, although the spinodal line may be smeared and not very sharp. Also, the structure factors under weak shear field must remain the same as the RPA form, which is probably a reasonable assumption.[20] Only under these three premises the extrapolation of linear region is reasonable to produce the "spinodal point" for noncritical polymer blends under shear mixing. By such a procedure we obtained the "spinodal points" for LPI20 and LPI80 at 53.1 ± 2.0 and 87.2 ± 2.0 °C at 0.25 rad/s, respectively. But the linear part in LPI40 and LPI60 is not obvious and can cause large errors; the acquired "spinodal temperatures" 54.8 ± 2.0 °C for LPI40 and 60.0 ± 2.0 °C for LPI60 at 0.25 rad/s are just for reference. It is understandable that the interfacial tension already take the dominant role in viscoelastic properties in our measurements. The linear regions with different ramp rates for LPI80 under frequency 0.25 and 1 rad/s cannot coincide, as shown in Figure 9a,b, and lead to different "spinodal points". The frequency dependence of LPI80 "spinodal points" is shown in Figure 10, in which the temperature ramping rates are all 1 °C/min, and the extrapolated quiescent "spinodal point" is 86.3 ± 2.0 °C. But we have to stress again that the extrapolated "spinodal points" have obvious temperature ramping rate dependence. Thus, the extrapolation to frequency 0 rad/s will probably produce a different "spinodal point" with the "true" quiescent "spinodal point". By closely examining the linear

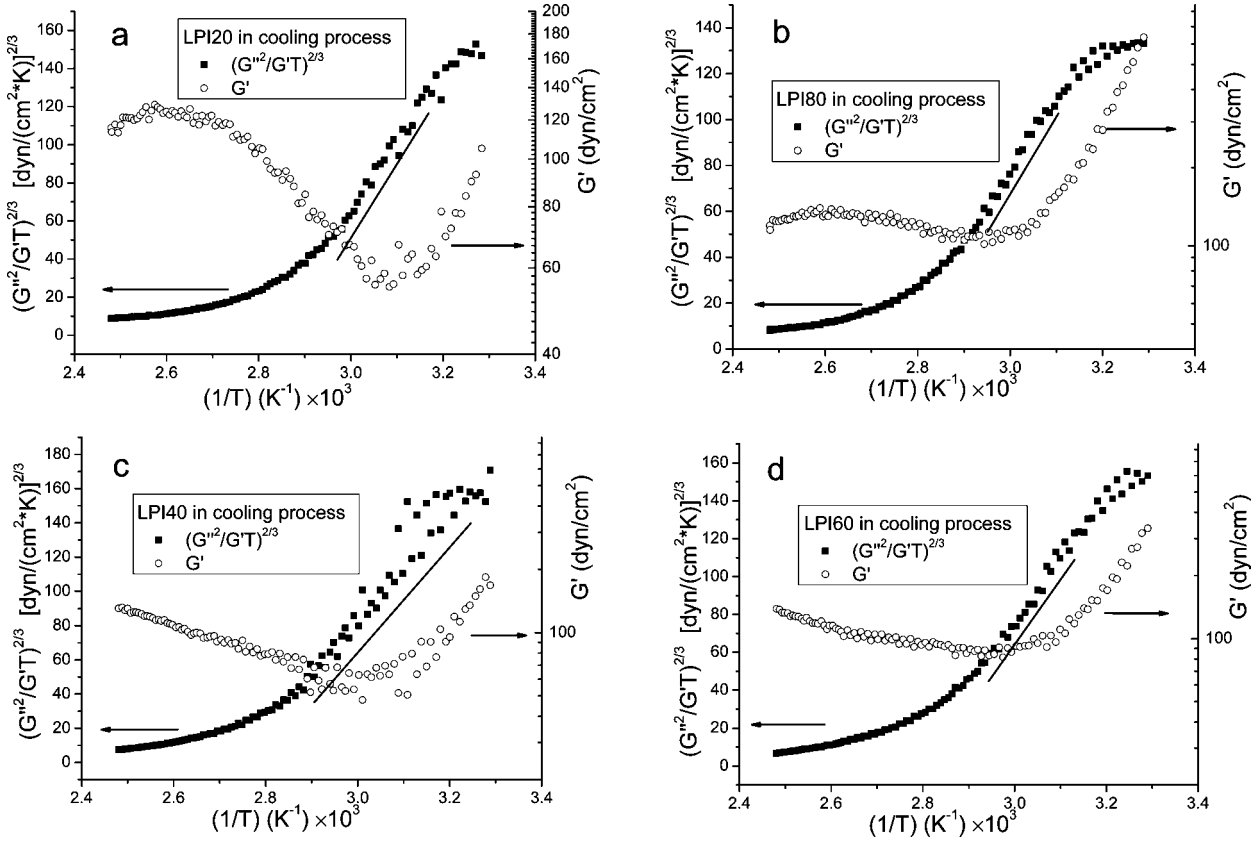

Figure 11. Storage modulus G' and the corresponding plots of $(G''^2/G'T)^{2/3}$ in cooling process vs $1/T \times 1000$ of (a) LPI20, (b) LPI80, (c) LPI40, and (d) LPI60.

regions in Figure 8a,b, we found that the linear regions correspond to the early stage of nucleation processes of LPI20 and LPI80, where the droplets volume are not too large to affect the RPA structure factors and the interfaces are not well developed yet. All the above results point to the fact that during the formation of nuclei the fluctuations may dominate the rheological behavior. Then the effect of fluctuations begins to decrease and interface emerges to take the dominant role in viscoelastic behavior.

Treatment of cooling process is not suitable to analyze the spinodal point because the RPA structure factor, which is used in the theoretical derivation, is completely not suitable for phase-separated samples. Surprisingly, the linear region existed in cooling process of every sample as shown in Figure 11a−d. The corresponding temperature regions of linear part is lower than that in the heating process for samples LPI20 and LPI80, but in samples LPI40 and LPI60 it shows opposite results. Again by comparing G' with $(G''^2/G'T)^{2/3}$ in the same X-axis, the linear parts always correspond to the gradual upturn of G'. A phenomenon like this may imply that in the process of crossing into the shear induced homogeneous state, interface is smeared and fluctuations dominate the viscoelastic behavior.

Conclusion

In a system of shear induced mixing with LCST type of phase diagram, we analyzed the rheological responses in the process of heating and cooling under low-frequency oscillatory shear. In the off-critical sample, LPI8, we discussed the effect of nucleation process on the viscoelastic behavior in metastable region with the consideration of the viscoelasticity models, together with fluctuations and some of the newly developed nucleation theory. We concluded that in the off-critical samples, like LPI80, the newly born nuclei droplets as well as the growth of the droplets will both help the increase of storage modulus G'. But after the crossing over of some critical size, the effect of growing droplet will actually cause a decrease of the G'. Whereas in the unstable region the situation is different, no new nuclei were produced and droplet size increases all the time while the interfacial tension changes only little. Thus, the storage modulus G' decreases all the time. Since all the measurements were carried out by ramping through the metastable region, instead of "quench" into the unstable region, for near-critical samples, like LPI60, three linear regions in G' vs T have been observed. These may be related to the morphological evolution, and more simultaneous microscopic work or scattering experiments are needed in the future. The physical origins of these two different types of rheological responses are probably due to the different morphological growth mechanisms in near- and off-critical samples and the phase separation kinetics in metastable and unstable regions. In order to check kinetics more closely, we did time-dependent experiments at different temperatures. The time scan results show that the time evolution for LPI80 type is only noticeable in nucleation and growth process which are not so prominent in the other temperature regions (metastable and unstable). While in LPI60 type the system is already in the unstable region at rheological test, the dynamical changes are fast and prominent in all the higher temperatures.

On the next step we used Ajji and Choplin's theory[38] to extrapolate to the "spinodal points" of our samples. This kind of generalization in noncritical compositions is based on three important hypotheses about fluctuations. The linear part in heating process coincides with the early stage of nucleation process. The data treatment in the cooling process showed that the linear region also existed and was controlled by the critical like fluctuations, which could correlate with the smearing of interface. It is clear that fluctuations have a significant influence on the viscoelastic measurements when interfaces are not well developed. More experiments are needed especially in conjunction with scattering and/or microscopy in order to better understand the phase separation kinetics under shear flow.

Acknowledgment. The author thanks the fund support of NSFC Projects 20490220 and 50773087. The authors also appreciate the useful discussion with Dr. X. Wang.

References and Notes

(1) de Gennes, P. G. *J. Chem. Phys.* **1980**, *72*, 4756–4763.
(2) Pincus, P. *J. Chem. Phys.* **1981**, *75*, 1996–2000.
(3) Binder, K. *J. Chem. Phys.* **1983**, *79*, 6387–6409.
(4) Nishi, T.; Wang, T. T.; Kwei, T. K. *Macromolecules* **1975**, *8*, 227–234.
(5) Sato, T.; Han, C. C. *J. Chem. Phys.* **1988**, *88*, 2057–2065.
(6) Okada, M.; Han, C. C. *J. Chem. Phys.* **1986**, *85*, 5317–5327.
(7) Jinnai, H.; Hasegawa, H.; Hashimoto, T.; Han, C. C. *Macromolecules* **1991**, *24*, 282–289.
(8) Hashimoto, T.; Itakura, M.; Hasegawa, H. *J. Chem. Phys.* **1986**, *85*, 6118–6128.
(9) Hashimoto, T.; Itakura, M.; Shimidzu, N. *J. Chem. Phys.* **1986**, *85*, 6773–6786.
(10) Hashimoto, T. *Phase Transitions* **1988**, *12*, 47–119.
(11) Balsara, N. P.; Rappl, T. J.; Lefebvre, A. A. *J. Polym. Sci., Part B: Polym. Phys.* **2004**, *42*, 1793–1809.
(12) Patel, A. J.; Balsara, N. P. *Macromolecules* **2007**, *40*, 1675–1683.
(13) Zhang, X. H.; Wang, Z. G.; Muthukumar, M.; Han, C. C. *Macromol. Rapid Commun.* **2005**, *26*, 1285–1288.
(14) Brown, G.; Chakrabarti, A. *J. Chem. Phys.* **1993**, *98*, 2451–2458.
(15) Heeley, E. L.; Poh, C. K.; Li, W.; Maidens, A.; Bras, W.; Dolbnya, I. P.; Gleeson, A. J.; Terrill, N. J.; Fairclough, J. P. A.; Olmsted, P. D.; Ristic, R. I.; Hounslow, M. J.; Ryan, A. J. *Faraday Discuss.* **2003**, *122*, 343–361.
(16) Zettlemoyer A. C. *Nucleation*; Marcel Dekker: New York, 1969.
(17) Wood, S. M.; Wang, Z. G. *J. Chem. Phys.* **2002**, *116*, 2289–2300.
(18) Wang, Z. G. *J. Chem. Phys.* **2002**, *117*, 481–500.
(19) Saito, S.; Koizumi, S.; Matsuzaka, K.; Suehiro, S.; Hashimoto, T. *Macromolecules* **2000**, *33*, 2153–2162.
(20) Hobbie, E. K.; Hair, D. W.; Nakatani, A. I.; Han, C. C. *Phys. Rev. Lett.* **1992**, *69*, 1951–1954.
(21) Gerard, H.; Higgins, J. S.; Clarke, N. *Macromolecules* **1999**, *32*, 5411–5422.
(22) Onuki, A.; Kawasaki, K. *Prog. Theor. Phys. Suppl.* **1978**, *64*, 436–441.
(23) Onuki, A.; Kawasaki, K. *Ann. Phys.* **1979**, *121*, 456–528.
(24) Onuki, A.; Yamazaki, K.; Kawasaki, K. *Ann. Phys.* **1981**, *131*, 217–242.
(25) Han, C. C.; Yao, Y. H.; Zhang, R. Y.; Hobbie, E. K. *Polymer* **2006**, *47*, 3271–3286.
(26) Kapnistos, M.; Hinrichs, A.; Vlassopoulos, D.; Anastasiadis, S. H.; Stammer, A.; Wolf, B. A. *Macromolecules* **1996**, *29*, 7155–7163.
(27) Kapnistos, M.; Vlassopoulos, D.; Anastasiadis, S. H. *Europhys. Lett.* **1996**, *34*, 513–518.
(28) Madbouly, S. A.; Ougizawa, T. *Macromol. Chem. Phys.* **2004**, *205*, 1222–1230.
(29) Niu, Y. H.; Wang, Z. G. *Macromolecules* **2006**, *39*, 4175–4183.
(30) Nesarikar, A. R. *Macromolecules* **1995**, *28*, 7202–7207.
(31) Kitade, S.; Takahashi, Y.; Noda, I. *Macromolecules* **1994**, *27*, 7397–7401.
(32) Poios, I. S.; Soliman, M.; Lee, C.; Gido, S. P.; Schmidt-Rohr, K.; Winter, H. H. *Macromolecules* **1997**, *30*, 4470–4480.
(33) Vinckier, I.; Laun, H. M. *Rheol. Acta* **1999**, *38*, 274–286.
(34) Weis, C.; Leukel, J.; Borkenstein, K.; Maier, D.; Gronski, W.; Friedrich, C.; Honerkamp, J. *Polym. Bull.* **1998**, *40*, 235–241.
(35) Castro, M. I.; Carrot, C.; Prochazka, F. *Polymer* **1999**, *45*, 4095–4104.
(36) Mani, S.; Malone, M. F.; Winter, H. H. *J. Rheol.* **1992**, *36*, 1625–1649.
(37) Stadler, R.; Freitas, L. L.; Krieger, V.; Klotz, S. *Polymer* **1988**, *29*, 1643–1647.
(38) Ajji, A.; Choplin, L. *Macromolecules* **1991**, *24*, 5221–5223.
(39) Fredrickson, G. H.; Larson, R. G. *J. Chem. Phys.* **1987**, *86*, 1553–1560.
(40) Palierne, J. F. *Rheol. Acta* **1990**, *29*, 204–214.
(41) Graebling, D.; Muller, R.; Palierne, J. F. *Macromolecules* **1993**, *26*, 320–329.
(42) Lee, H. M.; Park, O. O. *J. Rheol.* **1994**, *38*, 1405–1425.
(43) Bousmina, M. *Rheol. Acta* **1999**, *38*, 73–83.

(44) Jeon, H. S.; Nakatani, A. I.; Han, C. C.; Colby, R. H. *Macromolecules* **2000**, *33*, 9732–9739.
(45) Lacroix, C.; Aressy, M.; Carreau, P. J. *Rheol. Acta* **1997**, *36*, 416–428.
(46) Jeon, H. S.; Nakatani, A. I.; Hobbie, E. K.; Han, C. C. *Langmuir* **2001**, *17*, 3087–3095.
(47) Kielhorn, L.; Colby, R. H.; Han, C. C. *Macromolecules* **2000**, *33*, 2486–2496.
(48) Bousmina, M. *Rheol. Acta* **1999**, *38*, 251–254.
(49) Akcasu, A, Z.; Bahar, I.; Erman, B.; Feng, Y.; Han, C. C. *J. Chem. Phys.* **1992**, *97*, 5782–5793.

MA800646S